Energy Storage Materials 42 (2021) 78–87

Contents lists available at ScienceDirect

Energy Storage Materials

journal homepage: www.elsevier.com/locate/ensm

Role of electrolyte in stabilizing hard carbon as an anode for rechargeable sodium-ion batteries with long cycle life

Hayley S. Hirsh[a], Baharak Sayahpour[b], Ashley Shen[a], Weikang Li[a], Bingyu Lu[b], Enyue Zhao[a], Minghao Zhang[a,*], Ying Shirley Meng[a,b,*]

[a] Department of NanoEngineering, University of California, San Diego, La Jolla, CA 92121, USA
[b] Materials Science and Engineering Program, University of California, San Diego, La Jolla, CA 92121, USA

ARTICLE INFO

Keywords:
Sodium-ion batteries
Hard carbon anode
Electrode electrolyte interface
Grid-storage

ABSTRACT

Hard carbon (HC) is an attractive anode material for grid-level sodium-ion batteries (NIBs) due to the widespread availability of carbon, its high specific capacity, and low electrochemical working potential. However, the issues of low first cycle Coulombic efficiency and poor rate performance of HC need to be addressed for it to become a practical long-life solution for NIBs. These drawbacks appear to be electrolyte dependent, since ether-based electrolytes can largely improve the performance compared with carbonate electrolytes. An explanation for the mechanism behind these performance differences is critical for the rational design of highly reversible sodium storage. Combining gas chromatography, Raman spectroscopy, cryogenic transmission electron microscopy, and X-ray photoelectron spectroscopy, this work demonstrates that the solid electrolyte interphase (SEI) is the key difference between ether- and carbonated-based electrolyte, which determines the charge transfer kinetics and the extent of parasitic reactions. Although both electrolytes show no residual sodium stored in the HC bulk structure, the uniform and conformal SEI formed by the ether-based electrolyte enables improved cycle efficiency and rate performance. These findings highlight a pathway to achieve long-life grid-level NIBs using HC anodes through interfacial engineering.

1. Introduction

Low-cost and reliable energy storage is essential for a safe, stable, and sustainable electrical grid [1,2]. Sodium-ion batteries (NIBs) with Co and Ni free cathodes are one of the promising solutions for grid energy storage, considering elemental abundance and their environmentally benign nature [3,4]. While the energy density of NIB cathodes has increased over the years, the commercialization of NIBs for grid energy storage is hindered by the inferior electrochemical performance of sodium anode materials [3]. Graphite, a common anode material for conventional lithium-ion batteries (LIBs), is not applicable for NIBs due to its negligible reversible capacity in carbonate-based electrolytes [5]. Though glyme-based electrolytes enable reversible capacity of sodium in graphite through solvent co-intercalation, the capacity is limited to ~100 mAh/g, and the reaction potential increases to about 0.75 V vs. Na metal [6]. Alternative anode materials for NIBs include sodium metal which has the highest theoretical capacity (1166 mAh/g) and lowest reaction potential, but it has severe safety hazards and a short lifetime [7]. Alloy and conversion types of anodes, such as Sn and SnO_2, also have high capacity, yet poor lifetimes caused by large volumetric changes during electrochemical cycling [8,9]. Insertion compounds, such as $NiCoO_2O_4$ and TiO_2, have relatively high average voltages (>0.5 V vs Na^+/Na^0), which reduce the energy density of a full cell [10,11]. Other anode materials like soft carbon and reduced graphene oxide also have high average voltages and shortened lifetimes due to low first cycle Coulombic efficiencies (CEs) (less than 60%) [12,13]. A promising exception is hard carbon (HC), which has been widely investigated as an anode material for NIBs because it is relatively safe, has a high capacity (> 200 mAh/g), and has a low reaction potential near 0 V vs. Na^+/Na^0.

By definition, HC, also known as non-graphitizing carbon, cannot be converted into graphite through heat treatment. It contains regions of parallel groups of graphite-like layers with no long-range order that form voids between the groups of layers. An additional advantage is that HC can be sustainably synthesized from biomass precursors such as banana peels, corn husks, peanut shells, as well as polymer/plastic derivatives [14–18]. The HC bulk structure, governed by the synthesis conditions, determines its electrochemical properties and performance [19,20]. Previous research has discovered ways to optimize the HC bulk structure (defects, surface area, graphitic like regions, and voids) for maximum capacity, CE, lifetime, and lowest average voltage [19].

* Corresponding authors.
E-mail addresses: miz016@eng.ucsd.edu (M. Zhang), shirleymeng@ucsd.edu (Y.S. Meng).

https://doi.org/10.1016/j.ensm.2021.07.021
Received 19 April 2021; Received in revised form 23 June 2021; Accepted 14 July 2021
Available online 18 July 2021

Table 1
Summary of electrolytes and techniques used to characterize the SEI of HC in literature.

Electrolyte	Technique	Washed?	SOC	Rate	Citation
1 M $NaClO_4$ in PC 1 M $NaClO_4$ in EC.PC 1.1 1 M $NaClO_4$ in EC.PC 1.1 w/ 10% DMC 1 M $NaPF_6$ in EC.PC 1.1 w/ 10% DME	XPS peak fitting	DMC	sodiated	C/20	[30]
0.5 M NaBOB in TMP 1 M $NaPF_6$ in TMP	XPS peak positions	TMP	1 cycle	C/10	[27]
0.8 M $NaPF_6$ in DEGDME 0.8 M $NaPF_6$ in EC.DEC 1.1	XPS elemental content, SEM	DMC	15 cycles	C/6	[28]
1 M $NaPF_6$ in EC.DEC 1.1 1 M $NaClO_4$ in EC.DEC 1.1 1 M NaTFSI in EC.DEC 1.1 1 M NaFTFSI in EC.DEC 1.1 1 M NaFSI in EC.DEC 1.1	XPS peak fitting & elemental content	DMC	sodiated	C/20	[31]
3 M NaFSI in PC 3 M NaFSI in PC.EC	XPS peak fitting, TEM	PC	5 cycles	C/10	[32]
1 M $NaClO_4$ in PC 1 M $NaClO_4$ in PC w/ 0.5% FEC 1 M $NaClO_4$ in PC w/ 2% FEC 1 M $NaClO_4$ in PC w/ 10% FEC	XPS peak positions, SEM	Not listed	1 cycle	C/10	[33]
1 M $NaClO_4$ in PC.EC 1.1	XPS peak positions, SEM	Not listed	sodiated, desodiated	C/6	[34]
1 M $NaClO_4$ in PC	XPS peak positions, TOF-SIMS, TEM	Not listed	1 cycle	C/10	[35]
1 M $NaPF_6$ in PC 1 M $NaBF_4$ in TEGDME	XPS peak fitting & elemental content, SEM, EDS, Cryo-TEM	Washed with PC or TEGDME and Unwashed	sodiated, desodiated	C/3, C/10, C/20	This paper

Even with an optimized bulk structure, the low first cycle CE and poor rate capability of HC have hindered its use in NIB full cells. The first cycle CE of HC in high performing carbonate electrolyte is between 60-80% at a rate of C/20, and only ~30% of the capacity is retained at a higher rate [21]. A low first cycle CE limits the lifetime of a battery because it reduces the total amount of sodium available in the system. This is especially problematic for commercialized cells where the only sources of sodium are from the cathode material and the lean amount of electrolyte. In literature, it has been proposed that the low first cycle CE is a result of trapped sodium in the bulk structure [19,22,23]. In addition, a battery that has excellent rate capability is essential for grid storage applications. Solutions for grid storage handle power fluctuations, which would be severely impaired by a poor rate performing battery [24]. The origin of the poor rate capability is proposed to be dictated by the poor kinetics of sodium filling the HC structural voids during the plateau region of the voltage curve [19,25].

However, recent research suggests the first cycle CE and rate performance is not solely determined by the HC bulk structure but is also highly dependent on the choice of electrolyte [26]. For example, an HC anode with an ether-based electrolyte (1 M $NaBF_4$ in TEGDME) has shown a first cycle CE of 87% and a retention of 84% of its C/20 capacity at 2C [26]. Electrolyte is known to have a major role in the formation of the solid electrolyte interphase (SEI). An ideal SEI that inhibits parasitic reactions between the HC surface and the electrolyte should be thin, ionically conductive, conformal, and robust. These aspects can affect both the first cycle CE, through consumption of sodium-ions, and rate performance, through impedance at the interface. This raises the question that if the first cycle CE and rate capability are controlled by the HC bulk structure or by the SEI formation.

Properties of the SEI can vary with different electrolytes and electrochemical testing conditions. However, minimal research has been conducted on the formation of the SEI on HC, with most of the focus on carbonate-based electrolytes (summary in Table 1). Moreover, in the few studies that used non-carbonate electrolytes (TMP, DEGDME), the exact chemical composition and SEI morphology were not examined [27,28]. Previously, quantifying the consumption of Na^+ due to the SEI formation and observing the SEI's morphology at the nanoscale (HC is a beam-sensitive material) were very challenging. Due to the recently developed techniques such as titration gas chromatography (TGC) and cryogenic transmission electron microscopy (cryo-TEM), the SEI can now be better characterized [29].

In this study, we explored the origin of the first cycle CE and rate capability of HC in two electrolyte systems: conventional carbonate electrolyte and ether electrolyte. 1 M $NaPF_6$ in PC was chosen as the conventional carbonate electrolyte because it is one of the most common electrolytes used in NIB research. 1 M $NaBF_4$ in TEGDME was chosen as the ether electrolyte because recent studies have shown it improves HC's electrochemical performances [26]. Electrochemical testing, TGC, and *ex-situ* Raman spectroscopy were applied to observe the (de)sodiation processes and the reversibility of sodium stored in the HC bulk structure. Cryo-TEM, scanning electron microscopy (SEM), energy dispersive X-ray spectroscopy (EDS), and X-ray photoelectron spectroscopy (XPS) were used to characterize both the morphological and composition changes of the SEI for carbonate- and ether- based electrolytes at three different cycling rates. A long-term electrochemical study of HC in these two electrolytes was used to determine how the SEI formation affects the lifetime of the anode material. These techniques demonstrate that SEI is the dominant influence on both the first cycle CE and rate capability of HC.

2. Methods

2.1. Electrochemical Characterization

Composite anodes were prepared by mixing a slurry of 90.4 wt. % HC (Xiamen Tmax Battery Equipments Limited) and 9.06 wt. % carboxy methyl cellulose sodium salt (CMC) 250,00 MW with DI water as the solvent (characterization of pristine HC in **SI Fig. 1**). The slurry was cast onto aluminum foil and dried under vacuum at 80°C overnight. Na metal was used as the counter electrode. 1 M $NaPF_6$ in PC was used for the conventional carbonate electrolyte cells, and 1 M $NaBF_4$ in TEGDME was used for the ether-based electrolyte cells. For all cells, except those used for TGC measurements, 50 μL of electrolyte and one layer of glass fiber GF/F (Whatman) was used as the separator. Cells used for TGC measurements had 70 μL of electrolyte and two layers of glass fiber GF/F (Whatman) as the separator. Electrodes 14 mm in diameter with an active mass loading of 3.2-4.0 mg/cm^2 were assembled in 2032 coin cells in an argon-filled glove box (H_2O < 0.1 ppm) and tested on an Arbin battery cycler. Coin cells were allowed to rest 8 h before electrochemical tests were performed. The voltage range was maintained between 0.005V-2 V and the C-rates were calculated, assuming a theoretical specific capacity of 150 mAh/g. Electrochemical impedance spectroscopy

(EIS) was carried out with 10 mV perturbation and AC frequencies from 100 kHz to 1 mHz. A SP-150 Biologic Potentiostat was used to measure impedance after 1 cycle at a rate of C/3. An equivalent circuit model was used to fit and analyze the data using Zview software (v. 3.4a, Scribner Associates, Inc.)

2.2. Materials characterization

TGC was performed using a Shimadzu GC instrument equipped with a BID detector and using an ultra-high purity Helium (99.999%) as the carrier gas. The samples were prepared in an argon-filled glovebox (H_2O < 0.1 ppm). Each sample was immediately transferred to a glass flask after disassembling and sealed using a septum under Argon. Then, 0.5mL of ethanol was injected into the container to fully react with ionic and metallic sodium. After the reaction is completed, a 30 μL gas sample was taken from the container using a gastight Hamilton syringe and immediately injected into the GC. The amount of ionic and metallic sodium was quantified based on the amount of detected H_2 gas by the GC.

Raman spectroscopy was performed using Renishaw inVia Raman Microscope. The samples were sealed between two very thin transparent glass slides in an argon-filled glovebox (H_2O < 0.1 ppm). The measurements were run using a 532-nm laser source, 1800 l/mm grating, and x20 magnification.

The morphology of the electrodes was identified using an FEI Apreo SEM equipped with EDS operating at 3 kV. For the cryo-TEM sample preparation, a TEM grid was directly dropped into the pristine HC powders to pick up the particles. For the cycled HC particles, the sample particles were first dispersed in the corresponding electrolyte solvents (PC or TEGDME), then the particle suspension was dropped onto the TEM grid. The TEM grids with particle suspension were dried under vacuum overnight. Once dried, the sample grids were sealed in airtight bags before being transferred to the TEM facility. The grids were mounted onto a TEM cryo-holder (Gatan) via a cryo-transfer station. TEM characterizations were carried out on JEM-2100F at 200 kV.

XPS was performed using an AXIS Supra by Kratos Analytica. XPS electrode samples were disassembled and removed from their cells. Washed samples were washed with either PC or TEGDME and then dried under vacuum. Unwashed samples were directly dried under vacuum. The XPS was operated using an Al anode source at 15 kV, scanning with a step size of 0.1 eV and 200 ms dwell time. Fits of the XPS spectra were performed with CasaXPS software to identify the chemical composition of the surface of the electrodes.

3. Results and discussion

3.1. Electrochemical performance comparison with different electrolytes

Electrochemical measurements provide insight into the origin of the first cycle CE and rate capability of HC in PC electrolyte in comparison to that in TEGDME electrolyte. To investigate cycling rate dependence, HC was electrochemically tested at three different rates (C/20, C/10, and C/3). The results are shown in Fig. 1: 1) The HC cycled in the PC electrolyte has a lower first cycle CE than that in the TEGDME electrolyte at all rates (68.7% vs. 84.8% at C/3). This indicates that more sodium is trapped in the HC bulk structure or in the HC-SEI when cycled in PC electrolyte. 2) Overpotential increases significantly at faster rates for the PC electrolyte whereas the increase is less evident for the TEGDME electrolyte. This is exemplified by the differences of the plateau voltages, extracted from the low voltage peaks of the dQ/dV curves, for sodiation vs. desodiation as shown in **SI** Fig.2. Larger overpotentials imply either slower reaction kinetics of the bulk (de)sodiation mechanism or an increase of interface resistance in the PC electrolyte system. 3) Reversible capacity for the PC electrolyte decreases rapidly, from 247.5 mAh/g at C/20 to 112.4 mAh/g at C/3, whereas the reversible capacity for the TEGDME electrolyte only slightly decreases, from 268.1 mAh/g at C/20 to 259.0 mAh/g at C/3. The section of the HC-PC voltage curve most effected by the current rate is the plateau region (**SI Table 1**), corresponding to the void filling mechanism. The bulk structure and/or

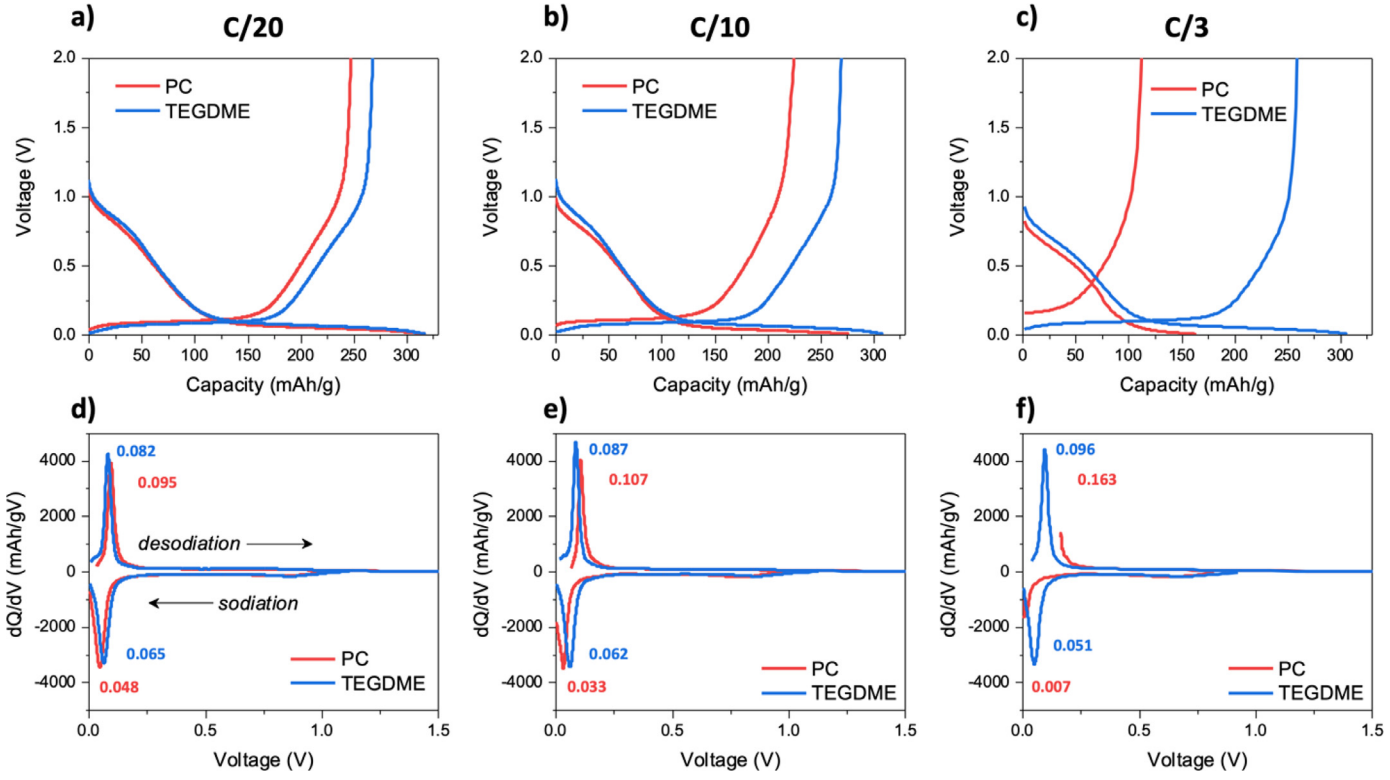

Fig. 1. First cycle voltage profiles and their corresponding differential voltage plots of HC with PC (red) or TEGDME electrolyte (blue) at a rate of (a, d) C/20, (b, e) C/10, and (c, f) C/3. The numbers highlighted in the differential voltage plots indicate the plateau voltages during (de)sodiation.

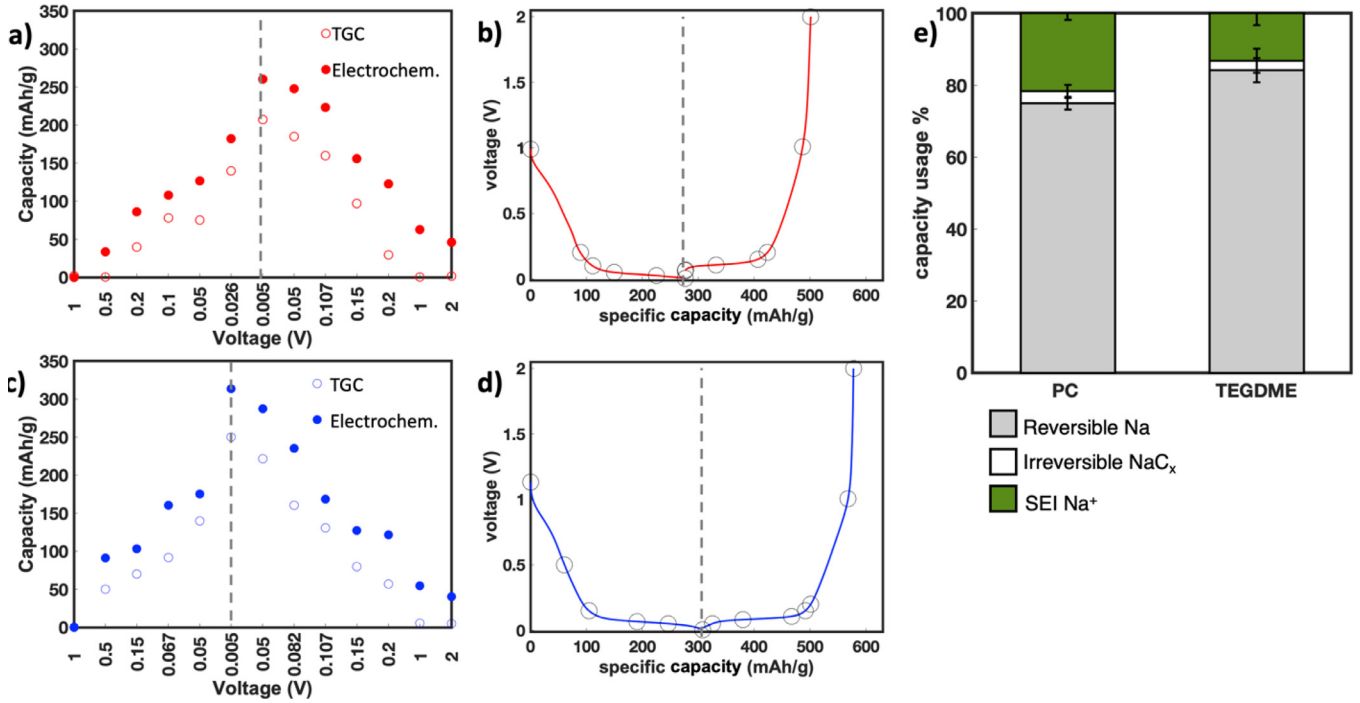

Fig. 2. Sodium stored in the HC at different states of charge with PC (a, b) or TEGDME electrolyte (c, d) measured by TGC (open circles) and electrochemistry (filled circles) with their representative voltage profiles tested at a rate of C/10. (e) Analysis of capacity usage, reversible Na, irreversible NaC_x, and SEI Na^+, for HC with PC and TEDGDME electrolyte using the TGC method. The error bars represent the standard deviation from the average values of the measured Na vs. SEI Na^+.

SEI formation phenomena are potentially responsible for the differences in the electrochemical performances of HC in the PC and the TEGDME electrolytes.

3.2. Sodiation/desodiation processes of HC

To investigate the irreversible sodium that controls the first cycle CE of HC, TGC was used to separate the contribution of sodium trapped in the HC bulk structure and the sodium in the SEI. This method was inspired by the Li metal TGC technique, first used to detect the mechanism of irreversible capacity for lithium plating/stripping [29]. The following reaction:

$$2Li + 2H_2O \rightarrow 2LiOH + H_2(g)$$

was applied to quantify the amount of residual metallic Li versus Li-containing compounds in the SEI on a stripped Li electrode. The TGC technique was also used to quantify the amount of Li inserted into a graphite anode [36]:

$$2LiC_x + 2H_2O \rightarrow 2LiOH + 2xC + H_2(g)$$

This method works by measuring the amount of H_2 gas to calculate the amount of Li stored in the graphite anode. The irreversible capacity, not contributed by irreversible Li in the graphite bulk structure, is ascribed to the SEI formation. These two types of irreversible lithium can be quantified because the SEI components do not react with water to form H_2 gas. In this study, ethanol was used as the titration solvent, because water could react with a possible SEI component, NaF, thereby forming HF. The potential reaction between HF and the aluminum current collector could then lead to the further generation of H_2 [37]. Possible components of the SEI, along with the pristine HC electrode, were tested with the TGC method and none reacted with ethanol to form H_2 (**SI Table 2 and SI** Fig. 3). It confirms that the H_2 gas is only produced by reacting ethanol with sodium (Na^0 and NaC_x) based on the following reactions:

$$2Na + 2CH_3CH_2OH \rightarrow 2(CH_3CH_2O^-Na^+) + H_2(g)$$

$$2NaC_x + 2CH_3CH_2OH \rightarrow 2(CH_3CH_2O^-Na^+) + 2xC + H_2(g)$$

The results of TGC tests are shown in Fig. 2, where the calculated amounts of Na stored in the HC bulk, referred to as NaC_x, at different states of charge in PC and TEGDME electrolytes are compared. Both the PC and the TEGDME electrolytes show a volcano-like shape where the amount of sodium calculated from the electrochemical capacity is always larger than the amount of sodium detected by TGC. This indicates that Na is involved in SEI formation throughout the first cycle. The amount of sodium that can be stored in the HC bulk structure, is NaC_{11} (theoretically $NaC_{8.0}$ for a capacity of 280 mAh/g) for PC and NaC_9 for TEGDME. Assuming the SEI formation process is highly irreversible, the increase in the amount of sodium stored in the HC bulk structure partially explains why TEGDME has a larger reversible capacity than PC. Additionally, there is negligible trapped sodium detected in the HC bulk structure after one cycle for both electrolytes. Unlike the Li metal deposition and stripping, residual sodium in the HC bulk structure is not the reason for the low first cycle CE. Instead, the first cycle CE of HC is more likely determined by the SEI formation process with Na inventory loss. The slight reduction of sodium utilized in the SEI upon desodiation could be due to partially reversible SEI species. This conclusion is also in agreement with the observation reported in literature that HCs with larger surface areas have lower first cycle CEs due to more interphase reactions [14,15,38–40].

The rate capability of HC has been proposed to be controlled by the kinetics of the sodium void filling mechanism, which occurs during the low voltage plateau [19,25]. If HC has similar (de)sodiation processes in the PC and TEGDME electrolytes, then it is unlikely that the kinetics of these processes control the rate capability of HC. Raman spectroscopy was used to study the (de)sodiation processes. As shown in Fig. 3, the Raman spectra of pristine HC contain two characteristic peaks termed the G and D bands. The G band (~1580 cm^{-1}) is characteristic of graphitic carbon and is related to the in-plane motion of the carbon atoms in graphene planes [41]. The D band (~1360 cm^{-1})

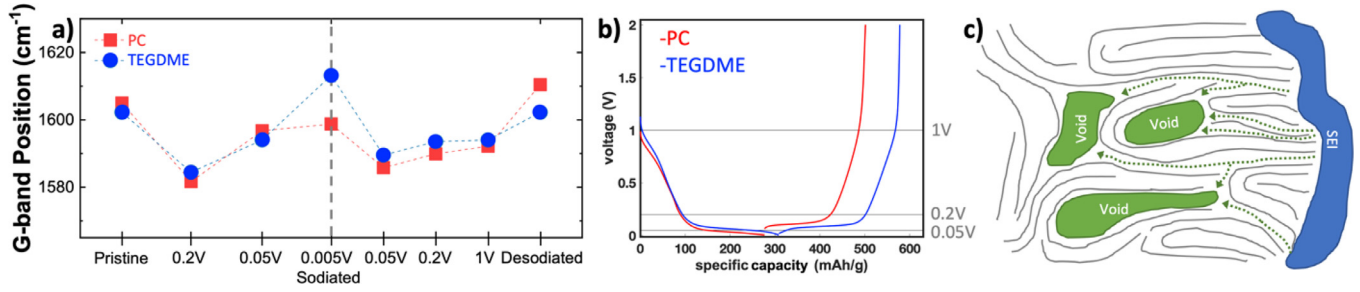

Fig. 3. Raman spectra (a) G-band positions and (b) representative voltage curves for HC with PC or TEGDME as the electrolyte tested at a rate of C/10. (c) A schematic showing the sodium pathway (green dotted arrows) through the graphitic region of the HC structure to reach the structural voids.

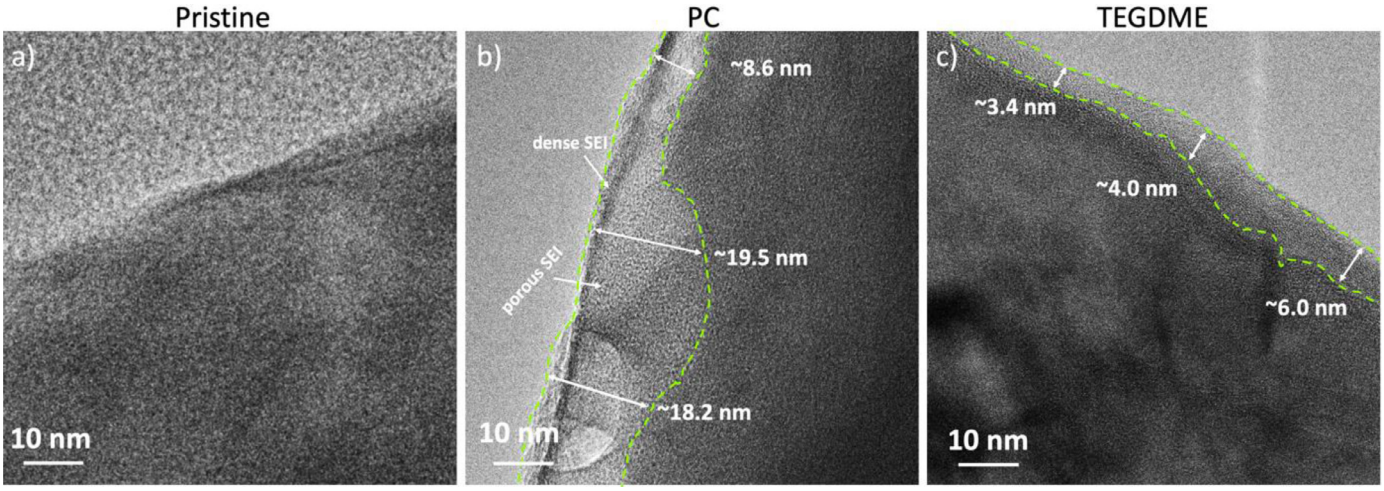

Fig. 4. Nano-scale structures of (a) pristine HC and HC after 1 cycle at a rate of C/3 in (b) PC and (c) TEGDME electrolyte imaged by cryo-TEM. The thickness of the SEI at various location is measured in the images.

is related to the presence of disorder or defects in the graphene planes [42]. The shift of these bands and/or the presence of a new peak can be induced by the (de)sodiation processes. An initial inspection of the TEGDME and PC samples (**SI** Fig. 4) reveals that the two characteristic peaks remain visible for both systems throughout the first cycle and that no other peaks manifest. This implies that: 1) the HC structure remains intact and 2) there is no intercalation staging since splitting of the G band is not present [43,44]. These observations are in agreement with the current understanding of the sodium storage mechanism in HC and indicate that both electrolytes elicit similar (de)sodiation processes.

In addition to the presence of the D and G bands, the position of the G band can reveal more information about the (de)sodiation processes (Fig. 3). The G band position is controlled by both charge transfer and lattice parameter changes in the graphitic regions [45]. For both samples, the G band position initially has a red shift for the slope region and then a blue shift for the voltage plateau region during sodiation. Upon desodiation, the reverse trend occurs. The initial red shift in the G band during the sloping region of sodiation indicates sodium insertion in the graphic regions [44]. The G band position reaches a minimum at the beginning of the voltage plateau region and a blue shift occurs as sodium fills the voids in the HC bulk structure (Fig. 3**(c)**) [46]. Given that there is a more significant blue shift of the G band for TEGDME sample upon maximum sodiation and that the plateau region has a larger capacity than the PC sample, ether-based electrolytes could enable an increase in HC void filling. This could be due to an increase in overpotential for the PC electrolyte, where less sodium can be stored in the voids at an equivalent cutoff voltage. Given the similar (de)sodiation processes for both PC and TEGDME electrolytes and the comparable Warburg coefficients of both systems (**SI** Fig. 5), which are related to the bulk diffusivity of sodium in HC, the rate performance of HC should not be solely determined by the kinetics of the bulk structure [52]. The formation of the SEI, as influenced by the choice of electrolyte and electrochemical conditions will thus be the focus of this study.

3.3. Morphology and composition of SEI with different electrolyte

The sodium consumption, resistance, and stability of an SEI are related to its morphology and chemical composition. The SEI morphology and elemental composition of HC with PC and TEGDME electrolytes were first explored by cryo-TEM, SEM, and EDS (Fig. 4 **and SI Figs. 6, 7, and 8**). In order to observe the nano-scale structure of the SEI by TEM, while preserving the intrinsic morphology of the SEI, cryogenic protection is required to minimize the beam damage. Clear differences in the SEI morphology on the irregularly shaped HC particles are observed for PC and TEGDME. The SEI formed in the PC electrolyte consists of a dense outer layer and a porous inner layer, whereas the SEI formed in the TEGDME electrolyte is uniformly dense around the whole HC particle. The SEI formed in the PC electrolyte morphology is also rate dependent, while the SEI formed in the TEGDME electrolyte is not (**SI** Fig. 7). At a rate of C/3, the SEI formed in the PC electrolyte is irregular, thick, and contains cracks, while at a rate of C/20 the SEI is thinner and more conformal. From cryo-TEM measurements, the thickness of formed SEI in the PC electrolyte at C/3 rate ranges from 10-20 nm whereas the SEI formed in the TEGDME is only 3-8 nm thick at the same C-rate. Additionally, EDS confirms that the SEI formed in the PC electrolyte contains significantly more sodium, oxygen, and fluorine than the SEI formed in the TEGDME electrolyte (**SI Fig. 8**). This, along with the cryo-TEM measurements, indicates that the SEI formed in the PC electrolyte could be the origin of sodium inventory lost that leads to the low first cycle CE.

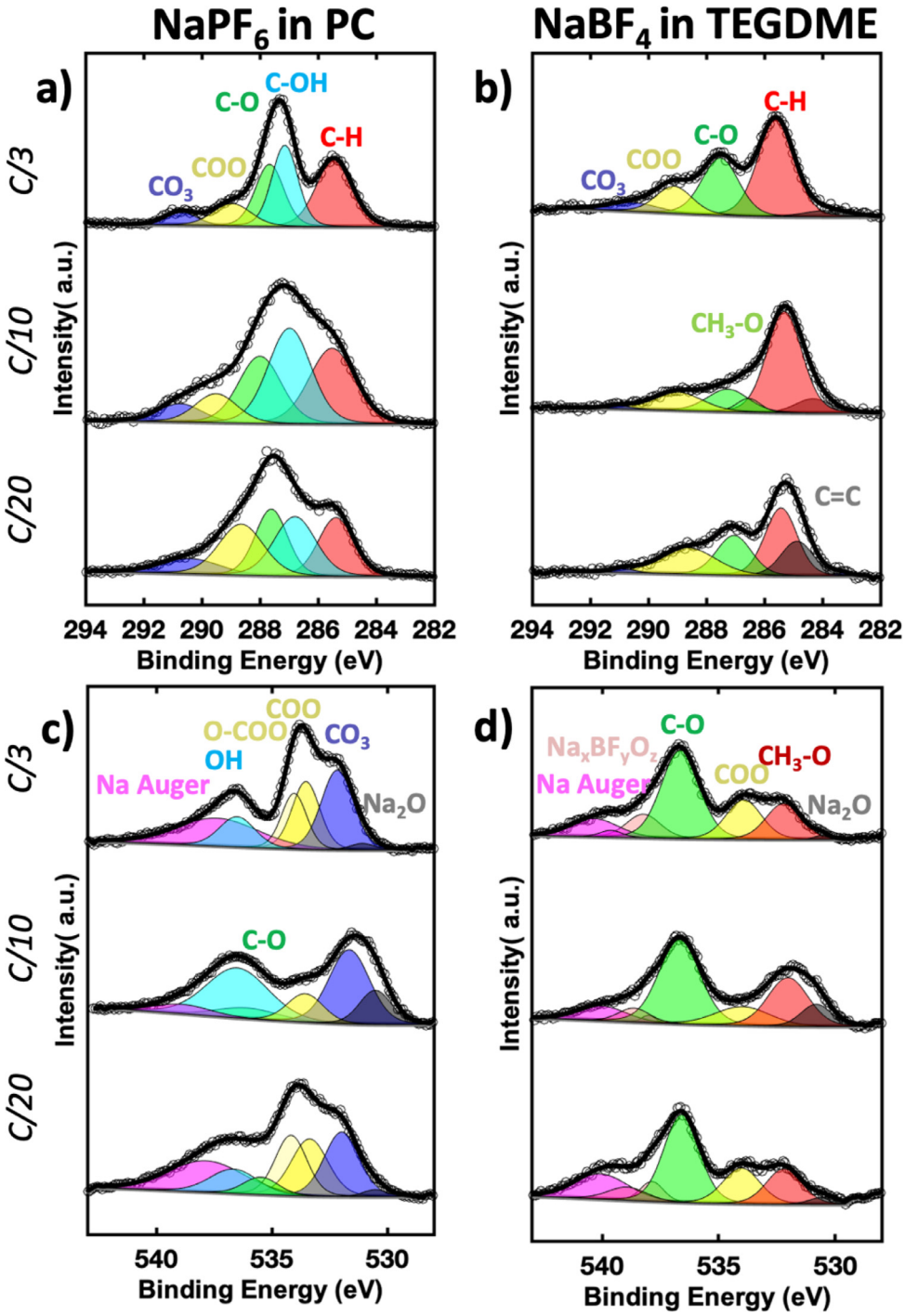

Fig. 5. (a, b) XPS C 1s regions and (c, d) XPS O 1s regions of HC cycled with PC (left) or TEGDME (right) electrolyte samples at different rates.

The actual chemical bonding environment that comprises the SEI has a critical effect on the sodium consumption and rate capability. XPS is one of the most common and useful tools for identifying the chemical bonding for elements that are contained in the SEI. It is essential that XPS samples are carefully prepared because the technique is surface sensitive and the SEI can be quite reactive. Past XPS studies prepared the SEI sample by washing it with a solvent, the intention of which was to remove the residue electrolyte salt. This preparation step can potentially disturb or damage the SEI prior to XPS measurements. As part of this study, we compared washed HC samples with unwashed samples and found that the act of washing actually removes fragile and/or reactive SEI components such as C-H, C-OH, CO_3, and Na_2O. This limits the observations of the SEI to the compounds remaining on the surface after washing, which obscures the changes between the sodiated and desodiated states of the HC SEI (**SI Fig. 9**). It is also important to note that the salt species do not overwhelm the signals for the unwashed samples (**SI Fig. 10**) which repudiates the arguments for washing XPS samples. We recommend that future XPS work on the characterization of HC and other anode SEIs should be performed on unwashed samples.

It is clear from comparing the sodiated and desodiated XPS spectra (**SI Fig. 9**) that for both PC and TEGDME electrolytes, the majority of the SEI is formed during the first sodiation process. Almost all the new chemical species, in comparison to the pristine electrode, appear in the sodiated spectra with minimal changes upon desodiation. The main difference between the sodiated and desodiated SEI is the relative amount of C-H bonding compared with other carbon bonds. Specifically, upon

desodiation, the C-H bond increases for both electrolytes. This suggests that the ester and ether species polymerized or that hydrocarbons are formed on the SEI during desodiation. The overall minimal changes for the SEIs upon desodiation support the hypothesis that the low first cycle CE, i.e., irreversible capacity, is mainly caused by SEI formation. Although SEI formed in the PC and TEGDME electrolytes are alike in primarily being formed during sodiation, their chemical species and relative amounts diverge.

The SEI formed in the PC electrolyte is mainly composed of alkyl/sodium carbonates (C-H, CO_3), polyesters (COO, O-COO, C-H), hydroxides (-OH), sodium fluoride (NaF), sodium oxide (Na_2O), and salt decomposition (Na_xPF_y). The SEI formed in the TEGDME electrolyte is composed of sodium alkoxides (CH_3-O, C-H), polyethers (C-O, C-H), sodium fluoride (NaF), sodium oxide (Na_2O), and salt decomposition ($Na_xBF_yO_z$). Solvent and salt (from the electrolyte) decomposition are the origin of these chemical species. PC can decompose through a ring opening reaction by single electron nucleophilic attack pathway to form a linear alkyl carbonate [47]. This molecule can then decompose into oxygen and propylene, which react with PC to produce polyesters. Sodium alkoxides and polyether are derived from the decomposition of TEGDME molecules.

The components of the SEI influence its stability and through studying these components we can better understand why the SEI formed in the PC electrolyte is more unstable than the SEI formed in the TEGDME electrolyte. The reaction pathway for the decomposition of PC, that eventually forms polyesters, can lead to continuous decomposition of PC molecules and does not form a compact and conformal morphology, as seen in the cryo-TEM images [47]. In addition, hydroxide groups are partially soluble in PC, which means they likely cause continual parasitic reactions. $NaPF_6$ has also been shown to react with an SEI component, sodium carbonate, to form CO_2 [31]. Gas formation from the PC and $NaPF_6$ decomposition can damage the SEI, especially one that contains brittle components, like sodium carbonate [48]. In addition, carbonate and polyester species are considered unfavorable for ion transport which can lead to larger overpotentials and poor electrochemical performance (**SI Table 3**). In contrast, TEGDME decomposition products, sodium alkoxides and polyethers, are already known to form superior, compact, thin, and stable SEIs on tin, bismuth, and rGO anodes [49–51]. This compact and elastic nature of alkoxides and polyethers can enable fast ion transport through the SEI [49–51]. The influence of the electrolyte on cell impedance was further evaluated by EIS (**SI Fig. 11**). The PC electrolyte resulted in both higher charge transfer resistance and resistance due to Na^+ diffusion through the SEI than the TEGDME electrolyte. The high resistance of the PC cell is likely caused by the thick SEI composed of chemical species with poor ionic transport properties, such as sodium carbonate and polyesters. In contrast, the stability and fast ionic transport of SEI components formed in the TEGDME electrolyte can enable superior battery lifetime and rate capability.

SEI formation and stability is controlled not only by the electrolyte, but also the rate of electrochemical cycling. This factor is especially important in investigating the HC system where the PC and TEGDME electrolytes have significantly different rate capabilities. The XPS spectra for the SEI formed in the PC and TEGDME electrolytes for three rates are shown in Fig. 5. Over the different rates, the SEI formed in the TEGDME electrolyte components have minimal changes whereas the SEI formed in the PC electrolyte composition varies. At a rate of C/3, the SEI formed in the PC electrolyte contains a larger amount of hydroxide groups (-OH) relative to ester (COO) and ether (CO) groups. Since hydroxide groups are partially soluble in PC, they are likely to cause continual parasitic reactions, which limits the lifetime of a battery at fast rates. As the rate slows, the composition of the SEI formed in the PC electrolyte becomes more similar to the composition of the SEI formed in the TEGDME electrolyte with a decrease of hydroxide groups and an increase in ether groups (CO). Ether groups are not soluble in PC and can form a more compact and therefore stable SEI. Other peaks, such as carbonate and C-H relative amounts, remain rate independent for the PC electrolyte. The SEI formed in the TEGDME electrolyte components and relative amounts appear to be rate independent. The one exception is a small carbonate peak, only identified in the C/3 SEI. The carbonate peak could be a result of an altered reaction at the faster rate or the detection of carbonate on the surface of HC due to a very thin SEI. The other consistent SEI components reveal that they are stable at slow and fast rates for TEGDME electrolyte. The compact and elastic nature of alkoxides and polyethers that compose the SEI formed in the TEGDME electrolyte enables fast ion transport at all rates [49–51].

3.4. Long-term cycling stability of HC

Long-term electrochemical HC studies were performed for the PC and TEGDME electrolytes where the first three cycles were run at a rate

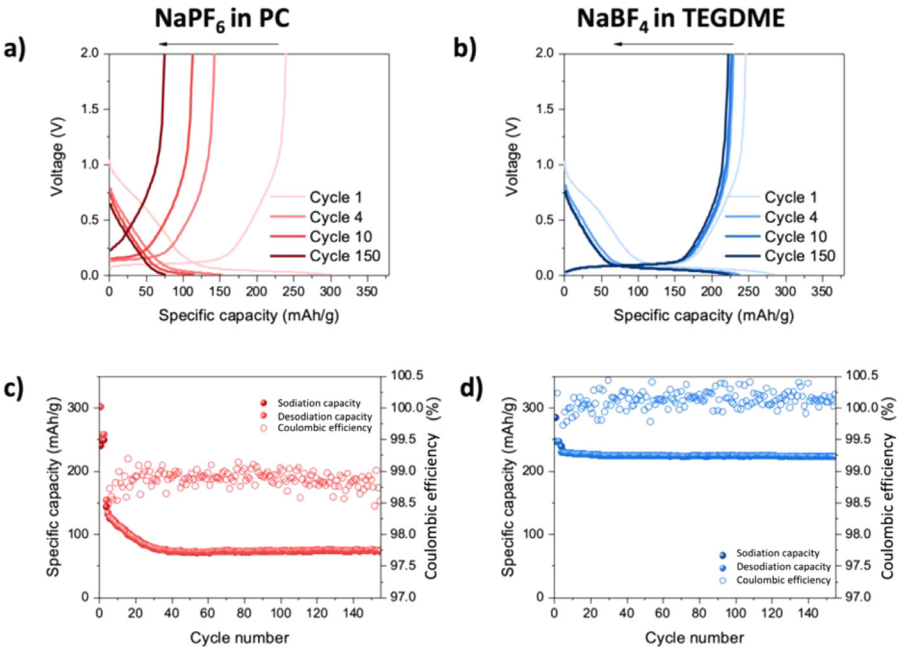

Fig. 6. (a, b) Voltage profiles and (c, d) specific capacity and CE vs. cycled number for HC in (left) PC or (right) TEGDME electrolyte.

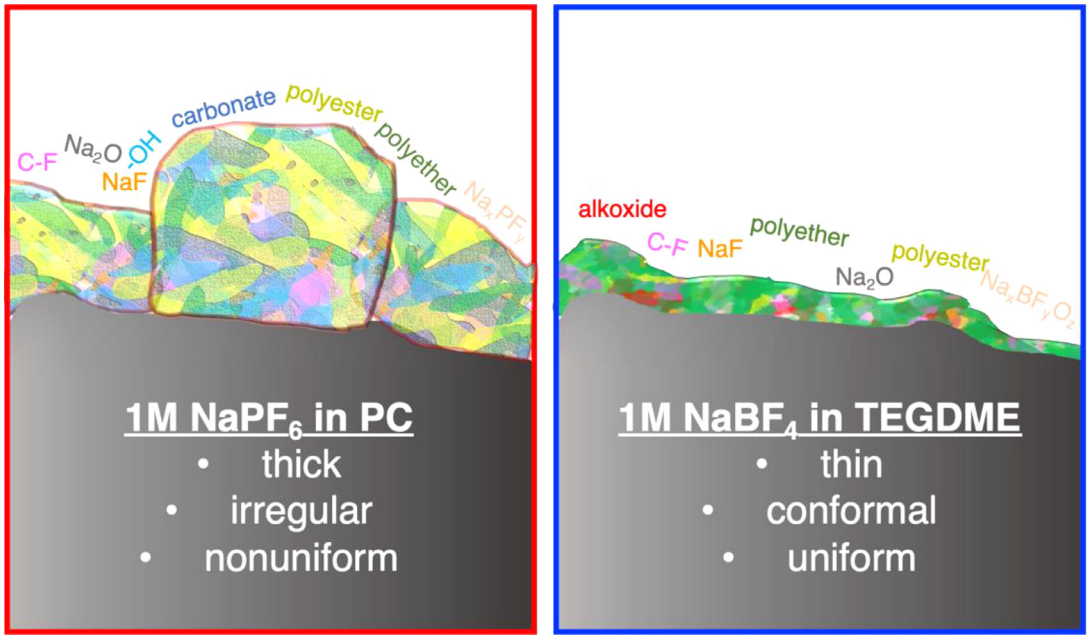

Fig. 7. Cross-sectional schematics of the differences between the SEI on HC in PC vs. TEGDME electrolyte.

of C/10 and the following cycles were operated at a rate of C/3 (Fig. 6). This mirrors how full cells are tested with the initial cycles run at a slower rate, known as formation cycles. The HC cell with PC electrolyte performs poorly, with a capacity of 74.9 mAh/g, CE of 98.7%, and a capacity retention of 31.6% after 150 cycles. The capacity of the cell with PC electrolyte rapidly declines during the first 50 cycles and then stabilizes. This, along with the relatively low average CE, shows that even the SEI formed with PC at a slower rate is unstable and leads to a poor lifetime at faster rates. In contrast, the HC cell with TEGDME electrolyte performs well, with a capacity of 222.9 mAh/g, average CE of 100.0%, and a capacity retention of 90.4% after 150 cycles. This shows that SEI formed in the TEGDME electrolyte is extremely stable at a faster rate and enables a long lifetime. The variations of the CE around 100% could be a result of temperature fluctuations during testing and/or potential SEI component reversibility.

3.5. Schematics for SEI with different electrolytes

The results from this study were combined into a schematic for the SEI formation on HC with PC and TEGDME electrolytes as shown in Fig. 7. This schematic illustrates the main chemical components, characteristics, and morphologies of the SEIs formed in PC and TEGDME electrolytes. The PC-based SEI is mainly composed of alkyl carbonates, polyesters, sodium fluoride, sodium oxide, and $NaPF_6$ decomposition products. This SEI appears thick, with nonuniform density and coverage, qualities which can promote continuous reactions that shorten the battery lifetime. In addition, this type of SEI inhibits sodium transport and becomes more unstable at high rates, limiting the HC rate capability. The TEGDME-based SEI is composed of sodium alkoxides, polyethers, sodium fluoride, sodium oxide, and $NaBF_4$ decomposition products. This thin, conformal, and uniform SEI enables cycling stability and fast sodium ion transport. This model is in contrast with the hypothesis proposed in literature in which trapped sodium in the HC bulk structure and slow kinetics of the voltage plateau (de)sodiation processes are considered as the causes for the low first cycle CE and poor rate capability, respectively. Adopting this model suggests shifting the research direction away from presodiating HC, in an effort to reduce the amount of trapped sodium in the HC structure, toward improving the SEI properties [22,23].

4. Conclusions

In this study, the performance and mechanistic differences of HC in a conventional carbonate electrolyte (1 M $NaPF_6$ in PC) and a high performing ether electrolyte (1 M $NaBF_4$ in TEGDME) are explored. The TEGDME electrolyte enables a higher first cycle CE, better rate performance, and improved lifetime of HC. The trapped sodium in the HC bulk structure, (de)sodiation processes, and SEI formation were examined to study the origin of these performance differences. It is found that similar (de)sodiation processes occur in PC and TEGDME system. In addition, there is no trapped sodium found in HC after the first cycle, which indicates that the first cycle CE and rate capability are not determined by the sodium storage process in the bulk structure. Thereafter, the SEI formation was explored during the first cycle at three different rates using cryo-TEM, SEM, EDS, and XPS. The growth of a thin, conformal, and uniform SEI in TEGDME electrolyte enables stable cycling behavior of HC under different current densities. This mechanistic understanding for the HC SEI can be potentially generalized to other carbonate- and ether-based electrolytes. HC with ether-based electrolytes has superior electrochemical performances but its compatibility with sodium cathodes should be further explored to enable a high-energy, long-life full cell. These findings demonstrate a new pathway through electrolyte design and interfacial engineering to further improve the electrochemical performances of the HC anode for grid-storage level NIBs.

Authors Contributions

H.S.H., M.Z., and Y.S.M. designed the experiments. H.S.H. and A.S. performed the electrochemical experiments. B.S. carried out the Raman and TGC experiments. B.L. conducted the cryo-EM. H.S.H. performed the SEM and EDX experiments and analysis. W.L. conducted XPS experiments. Y.S.M, M.Z., and E.Z. supervised the research. H.H. wrote the manuscript. All authors contributed to the discussion and provided feedback on the manuscript.

Declaration of Competing Interest

The authors declare no conflict of interest.

Acknowledgments

We are grateful for the financial support from the USA National Science Foundation (NSF) under Award Number DMR1608968. The authors acknowledge the use of facilities and instrumentation supported by NSF through the UC San Diego Materials Research Science and Engineering Center (UCSD MRSEC), DMR-2011924. The SEM analysis in this work was performed at the San Diego Nanotechnology Infrastructure (SDNI), a member of the National Nanotechnology Coordinated Infrastructure, which is supported by the National Science Foundation (grant ECCS1542148). TEM and XPS were performed at the UC Irvine Materials Research Institute (IMRI). We would like to thank Dr. Ich Tran for his help with the XPS experiments at the University of California, Irvine Materials Research Institute (IMRI) using instrumentation funded in part by the National Science Foundation Major Research Instrumentation Program under grant no. CHE-1338173.

Supplementary materials

Supplementary material associated with this article can be found, in the online version, at doi:10.1016/j.ensm.2021.07.021.

References

[1] B. Dunn, B. Dunn, H. Kamath, J. Tarascon, Electrical energy storage for the gridfor the Grid : a Battery of choices, Sci. Mag. 334 (2011) 928–936, doi:10.1126/science.1212741.
[2] P.C.K. Vesborg, T.F. Jaramillo, Addressing the terawatt challenge: scalability in the supply of chemical elements for renewable energy, RSC Adv. 2 (2012) 7933, doi:10.1039/c2ra20839c.
[3] H.S. Hirsh, Y. Li, D.H.S. Tan, M. Zhang, E. Zhao, Y.S. Meng, Sodium-Ion Batteries Paving the Way for Grid Energy Storage, Adv. Energy Mater. 10 (2020) 1–8, doi:10.1002/aenm.202001274.
[4] Y. Kim, K.H. Ha, S.M. Oh, K.T. Lee, High-capacity anode materials for sodium-ion batteries, Chem. - A Eur. J. 20 (2014) 11980–11992, doi:10.1002/chem.201402511.
[5] B. Jache, J.O. Binder, T. Abe, P. Adelhelm, A comparative study on the impact of different glymes and their derivatives as electrolyte solvents for graphite co-intercalation electrodes in lithium-ion and sodium-ion batteries, Phys. Chem. Chem. Phys. 18 (2016) 14299–14316, doi:10.1039/c6cp00651e.
[6] B. Jache, P. Adelhelm, Use of graphite as a highly reversible electrode with superior cycle life for sodium-ion batteries by making use of co-intercalation phenomena, Angew. Chemie - Int. Ed. 53 (2014) 10169–10173, doi:10.1002/anie.201403734.
[7] C. Bao, B. Wang, P. Liu, H. Wu, Y. Zhou, D. Wang, H. Liu, S. Dou, Solid Electrolyte Interphases on Sodium Metal Anodes, Adv. Funct. Mater. 2004891 (2020) 1–27. doi:10.1002/adfm.202004891.
[8] Z. Li, J. Ding, D. Mitlin, Tin and Tin Compounds for Sodium Ion Battery Anodes: Phase Transformations and Performance, Acc. Chem. Res. 48 (2015) 1657–1665, doi:10.1021/acs.accounts.5b00114.
[9] V.S.A. Piriya, R.C. Shende, G.M. Seshadhri, D. Ravindar, S. Biswas, S. Loganathan, T.S. Balasubramanian, K. Rambabu, M. Kamaraj, S. Ramaprabhu, Synergistic Role of Electrolyte and Binder for Enhanced Electrochemical Storage for Sodium-Ion Battery, ACS Omega 3 (2018) 9945–9955, doi:10.1021/acsomega.8b01407.
[10] M. Islam, M.G. Jeong, J.Y. Hwang, I.H. Oh, Y.K. Sun, H.G. Jung, Self-assembled nickel-cobalt oxide microspheres from rods with enhanced electrochemical performance for sodium ion battery, Electrochim. Acta. 258 (2017) 220–227, doi:10.1016/j.electacta.2017.10.114.
[11] L. Ling, Y. Bai, Z. Wang, Q. Ni, G. Chen, Z. Zhou, C. Wu, Remarkable Effect of Sodium Alginate Aqueous Binder on Anatase TiO2 as High-Performance Anode in Sodium Ion Batteries, ACS Appl. Mater. Interfaces. 10 (2018) 5560–5568, doi:10.1021/acsami.7b17659.
[12] W. Luo, Z. Jian, Z. Xing, W. Wang, C. Bommier, M.M. Lerner, X. Ji, Electrochemically expandable soft carbon as anodes for Na-ion batteries, ACS Cent. Sci. 1 (2015) 516–522, doi:10.1021/acscentsci.5b00329.
[13] J. Zhao, Y.Z. Zhang, F. Zhang, H. Liang, F. Ming, H.N. Alshareef, Z. Gao, Partially Reduced Holey Graphene Oxide as High Performance Anode for Sodium-Ion Batteries, Adv. Energy Mater. (2018) 1803215, doi:10.1002/aenm.201803215.
[14] E.M. Lotfabad, J. Ding, K. Cui, A. Kohandehghan, W.P. Kalisvaart, M. Hazelton, D. Mitlin, High-density sodium and lithium ion battery anodes from banana peels, ACS Nano 8 (2014) 7115–7129, doi:10.1021/nn502045y.
[15] P. Liu, Y. Li, Y.S. Hu, H. Li, L. Chen, X. Huang, A waste biomass derived hard carbon as a high-performance anode material for sodium-ion batteries, J. Mater. Chem. A. 4 (2016) 13046–13052, doi:10.1039/c6ta04877c.
[16] W. Lv, F. Wen, J. Xiang, J. Zhao, L. Li, L. Wang, Z. Liu, Y. Tian, Peanut shell derived hard carbon as ultralong cycling anodes for lithium and sodium batteries, Electrochim. Acta. 176 (2015) 533–541, doi:10.1016/j.electacta.2015.07.059.
[17] Y. Bai, Z. Wang, C. Wu, R. Xu, F. Wu, Y. Liu, H. Li, Y. Li, J. Lu, K. Amine, Hard carbon originated from polyvinyl chloride nanofibers as high-performance anode material for Na-ion battery, ACS Appl. Mater. Interfaces. 7 (2015) 5598–5604, doi:10.1021/acsami.5b00861.
[18] Y. Cao, L. Xiao, M.L. Sushko, W. Wang, B. Schwenzer, J. Xiao, Z. Nie, L.V. Saraf, Z. Yang, J. Liu, Sodium ion insertion in hollow carbon nanowires for battery applications, Nano Lett 12 (2012) 3783–3787, doi:10.1021/nl3016957.
[19] X. Dou, I. Hasa, D. Saurel, C. Vaalma, L. Wu, D. Buchholz, D. Bresser, S. Komaba, S. Passerini, Hard carbons for sodium-ion batteries: Structure, analysis, sustainability, and electrochemistry, Mater. Today. 23 (2019) 87–104, doi:10.1016/j.mattod.2018.12.040.
[20] K. Kubota, S. Shimadzu, N. Yabuuchi, S. Tominaka, S. Shiraishi, M. Abreu-Sepulveda, A. Manivannan, K. Gotoh, M. Fukunishi, M. Dahbi, S. Komaba, Structural Analysis of Sucrose-Derived Hard Carbon and Correlation with the Electrochemical Properties for Lithium, Sodium, and Potassium Insertion, Chem. Mater. 32 (2020) 2961–2977, doi:10.1021/acs.chemmater.9b05235.
[21] A. Ponrouch, E. Marchante, M. Courty, J.M. Tarascon, M.R. Palac??n, In search of an optimized electrolyte for Na-ion batteries, Energy Environ. Sci. 5 (2012) 8572–8583, doi:10.1039/c2ee22258b.
[22] M. Liu, J. Zhang, S. Guo, B. Wang, Y. Shen, X. Ai, H. Yang, J. Qian, Chemically Presodiated Hard Carbon Anodes with Enhanced Initial Coulombic Efficiencies for High-Energy Sodium Ion Batteries, ACS Appl. Mater. Interfaces. 12 (2020) 17620–17627, doi:10.1021/acsami.0c02230.
[23] J. Tang, D.K. Kye, V.G. Pol, Ultrasound-assisted synthesis of sodium powder as electrode additive to improve cycling performance of sodium-ion batteries, J. Power Sources. 396 (2018) 476–482, doi:10.1016/j.jpowsour.2018.06.067.
[24] D.M. Davies, M.G. Verde, O. Mnyshenko, Y.R. Chen, R. Rajeev, Y.S. Meng, G. Elliott, Combined economic and technological evaluation of battery energy storage for grid applications, Nat. Energy. 4 (2019) 42–50, doi:10.1038/s41560-018-0290-1.
[25] K. Kubota, S. Komaba, Review—Practical Issues and Future Perspective for Na-Ion Batteries, J. Electrochem. Soc. 162 (2015) A2538–A2550, doi:10.1149/2.0151514jes.
[26] K. Du, C. Wang, L.U. Subasinghe, S.R. Gajella, M. Law, A. Rudola, P. Balaya, A comprehensive study on the electrolyte, anode and cathode for developing commercial type non-flammable sodium-ion battery, Energy Storage Mater 29 (2020) 287–299, doi:10.1016/j.ensm.2020.04.021.
[27] R. Mogensen, S. Colbin, A.S. Menon, E. Björklund, R. Younesi, Sodium Bis(oxalato)borate in Trimethyl Phosphate: A Fire-Extinguishing, Fluorine-Free, and Low-Cost Electrolyte for Full-Cell Sodium-Ion Batteries, ACS Appl. Energy Mater. 3 (2020) 4974–4982, doi:10.1021/acsaem.0c00522.
[28] P. Bai, Y. He, P. Xiong, X. Zhao, K. Xu, Y. Xu, Long cycle life and high rate sodium-ion chemistry for hard carbon anodes, Energy Storage Mater 13 (2018) 274–282, doi:10.1016/j.ensm.2018.02.002.
[29] C. Fang, J. Li, M. Zhang, Y. Zhang, F. Yang, J.Z. Lee, M.-H. Lee, J. Alvarado, M.A. Schroeder, Y. Yang, B. Lu, N. Williams, M. Ceja, L. Yang, M. Cai, J. Gu, K. Xu, X. Wang, Y.S. Meng, Quantifying inactive lithium in lithium metal batteries, Nature 572 (2019) 511–515, doi:10.1038/s41586-019-1481-z.
[30] A. Ponrouch, R. Dedryvère, D. Monti, A.E. Demet, J.M. Ateba Mba, L. Croguennec, C. Masquelier, P. Johansson, M.R. Palacín, Towards high energy density sodium ion batteries through electrolyte optimization, Energy Environ. Sci. 6 (2013) 2361–2369, doi:10.1039/c3ee41379a.
[31] G.G. Eshetu, T. Diemant, M. Hekmatfar, S. Grugeon, R.J. Behm, S. Laruelle, M. Armand, S. Passerini, Impact of the electrolyte salt anion on the solid electrolyte interphase formation in sodium ion batteries, Nano Energy 55 (2019) 327–340, doi:10.1016/j.nanoen.2018.10.040.
[32] J. Patra, H.T. Huang, W. Xue, C. Wang, A.S. Helal, J. Li, J.K. Chang, Moderately concentrated electrolyte improves solid–electrolyte interphase and sodium storage performance of hard carbon, Energy Storage Mater 16 (2019) 146–154, doi:10.1016/j.ensm.2018.04.022.
[33] S. Komaba, T. Ishikawa, N. Yabuuchi, W. Murata, A. Ito, Y. Ohsawa, Fluorinated ethylene carbonate as electrolyte additive for rechargeable Na batteries, ACS Appl. Mater. Interfaces. 3 (2011) 4165–4168, doi:10.1021/am200973k.
[34] K.L. Hong, L. Qie, R. Zeng, Z.Q. Yi, W. Zhang, D. Wang, W. Yin, C. Wu, Q.J. Fan, W.X. Zhang, Y.H. Huang, Biomass derived hard carbon used as a high performance anode material for sodium ion batteries, J. Mater. Chem. A. 2 (2014) 12733–12738, doi:10.1039/c4ta02068e.
[35] S. Komaba, W. Murata, T. Ishikawa, N. Yabuuchi, T. Ozeki, T. Nakayama, A. Ogata, K. Gotoh, K. Fujiwara, Electrochemical Na Insertion and Solid Electrolyte Interphase for Hard-Carbon Electrodes and Application to Na-Ion Batteries, Adv. Funct. Mater. 21 (2011) 3859–3867, doi:10.1002/adfm.201100854.
[36] E.J. McShane, E.J. McShane, A.M. Colclasure, D.E. Brown, D.E. Brown, Z.M. Konz, Z.M. Konz, K. Smith, B.D. McCloskey, B.D. McCloskey, Quantification of Inactive Lithium and Solid-Electrolyte Interphase Species on Graphite Electrodes after Fast Charging, ACS Energy Lett 5 (2020) 2045–2051, doi:10.1021/acsenergylett.0c00859.
[37] J. Petrovic, G. Thomas, Reaction of Aluminum with Water to Produce Hydrogen, 2010.
[38] C. Bommier, W. Luo, W.Y. Gao, A. Greaney, S. Ma, X. Ji, Predicting capacity of hard carbon anodes in sodium-ion batteries using porosity measurements, Carbon N. Y. 76 (2014) 165–174, doi:10.1016/j.carbon.2014.04.064.
[39] Y. Zheng, Y. Wang, Y. Lu, Y.S. Hu, J. Li, A high-performance sodium-ion battery enhanced by macadamia shell derived hard carbon anode, Nano Energy 39 (2017) 489–498, doi:10.1016/j.nanoen.2017.07.018.
[40] C. Matei Ghimbeu, J. Górka, V. Simone, L. Simonin, S. Martinet, C. Vix-Guterl, Insights on the Na+ion storage mechanism in hard carbon: Discrimination between the porosity, surface functional groups and defects, Nano Energy 44 (2018) 327–335, doi:10.1016/j.nanoen.2017.12.013.
[41] M. Inaba, H. Yoshida, Z. Ogumi, In situ Roman Study of Electrochemical Lithium Insertion into Mesocarbon Microbeads Heat-Treated at Various Temperatures, J. Electrochem. Soc. 143 (1996) 2572–2578, doi:10.1149/1.1837049.

[42] A. Raj K, M.R. Panda, D.P. Dutta, S. Mitra, Bio-derived mesoporous disordered carbon: An excellent anode in sodium-ion battery and full-cell lab prototype, Carbon N. Y. 143 (2019) 402–412, doi:10.1016/j.carbon.2018.11.038.
[43] S. Maruyama, T. Fukutsuka, K. Miyazaki, T. Abe, In situ Raman spectroscopic analysis of solvent co-intercalation behavior into a solid electrolyte interphase-covered graphite electrode, J. Appl. Electrochem. 49 (2019) 639–646, doi:10.1007/s10800-019-01312-3.
[44] C. Sole, N.E. Drewett, L.J. Hardwick, Insitu Raman study of lithium-ion intercalation into microcrystalline graphite, Faraday Discuss 172 (2014) 223–237, doi:10.1039/c4fd00079j.
[45] C.T. Chan, K.M. Ho, W.A. Kamitakahara, Zone-center phonon frequencies for graphite and graphite intercalation compounds: Charge-transfer and intercalate-coupling effects, Phys. Rev. B. 36 (1987) 3499–3502, doi:10.1103/PhysRevB.36.3499.
[46] M. Anji Reddy, M. Helen, A. Groß, M. Fichtner, H. Euchner, Insight into Sodium Insertion and the Storage Mechanism in Hard Carbon, ACS Energy Lett 3 (2018) 2851–2857, doi:10.1021/acsenergylett.8b01761.
[47] K. Pan, H. Lu, F. Zhong, X. Ai, H. Yang, Y. Cao, Understanding the Electrochemical Compatibility and Reaction Mechanism on Na Metal and Hard Carbon Anodes of PC-Based Electrolytes for Sodium-Ion Batteries, ACS Appl. Mater. Interfaces. 10 (2018) 39651–39660, doi:10.1021/acsami.8b13236.
[48] J. Huang, X. Guo, X. Du, X. Lin, J.-Q. Huang, H. Tan, Y. Zhu, B. Zhang, Nanostructures of solid electrolyte interphases and their consequences for microsized Sn anodes in sodium ion batteries, Energy Environ. Sci. 12 (2019) 1550–1557, doi:10.1039/c8ee03632b.
[49] B. Zhang, G. Rousse, D. Foix, R. Dugas, D.A.D. Corte, J.M. Tarascon, Microsized Sn as Advanced Anodes in Glyme-Based Electrolyte for Na-Ion Batteries, Adv. Mater. 28 (2016) 9824–9830, doi:10.1002/adma.201603212.
[50] C. Wang, L. Wang, F. Li, F. Cheng, J. Chen, Bulk Bismuth as a High-Capacity and Ultralong Cycle-Life Anode for Sodium-Ion Batteries by Coupling with Glyme-Based Electrolytes, Adv. Mater. 29 (2017) 1–7, doi:10.1002/adma.201702212.
[51] J. Zhang, D.W. Wang, W. Lv, S. Zhang, Q. Liang, D. Zheng, F. Kang, Q.H. Yang, Achieving superb sodium storage performance on carbon anodes through an ether-derived solid electrolyte interphase, Energy Environ. Sci. 10 (2017) 370–376, doi:10.1039/c6ee03367a.
[52] H. Xia, L. Lu, Li diffusion in spinel LiNi0.5Mn1.5O4 thin films prepared by pulsed laser deposition, Phys. Scr. T. T129 (2007) 43–48, doi:10.1088/0031-8949/2007/T129/010.